Digital Discovery

Accepted Manuscript

This article can be cited before page numbers have been issued, to do this please use: C. Fyfe, S. Yu and M. Reid, *Digital Discovery*, 2026, DOI: 10.1039/D6DD00065G.

ROYAL SOCIETY OF CHEMISTRY

rsc.li/digitaldiscovery

View Article Online
DOI: 10.1039/D6DD00065G

Journal Name

ARTICLE TYPE

Cite this: DOI: 00.0000/xxxxxxxxxx

When Chemistry is Too Colourful: Gamut Clipping in 8-bit sRGB Risks Misinterpretation of Camera-Based Chemical Analysis†

Calum Fyfe[a], Shengkai Yu[b], and Marc Reid*[a]

Received Date
Accepted Date

DOI: 00.0000/xxxxxxxxxx

Digital cameras are increasingly utilised to capture visual changes in chemical processes. Monitoring colour with computer vision tools serves as a valuable proxy for monitoring bulk chemical changes. Most consumer-grade cameras digitise the colours captured using the 8-bit sRGB colour space. Despite its ubiquity, it restricts the range of colour information that can be stored. With regards to chemical analysis and process monitoring, the limitations of using the 8-bit sRGB gamut have not been addressed. When real-world vivid colours one attempts to record lie outside the bounds of 8-bit sRGB, the digitisation of those colours can result in distortion, clipping, or loss of chemically relevant colour data. Ultimately, these sRGB gamut limitations risk the chemist misinterpreting the data they collect from a camera. In this paper, we examined the visible spectrum of a series of common dyes, and determined their colours spectroscopically, without the limitation of 8-bit sRGB encoding. We investigated how 8-bit sRGB encoding affects the interpretation of time-series data from theoretical colour changes in five dyes. Highly saturated chemical samples exceeded the 8-bit sRGB colour gamut, causing colour distortions and structural breaks in reaction-monitoring time series data, risking misinterpretation as kinetic phenomena of genuine chemical origin. Our findings underscore the importance of paying close attention to colour representation in digital chemistry. We offer practical guidance for researchers using and interpreting colour data for use in computer vision method development.

1 Introduction

In chemical research, visual changes are increasingly quantified by computer vision methods.[1–3] By-eye, these visual changes can serve as intuitive and qualitative indicators of process successful, failure, and progress. By using cameras to complement our eyes as part of modern digital chemistry and lab automation workflows, quantitative insights can be derived from the richness of visual information that can otherwise remain underutilized.[4–9] Visual changes indicate shifts in chemical and physical states, making them informative across many applications: pH changes, chromic material responses, peptide synthesis, catalysis, mixing analysis, forensic spot test, turbidity profiling, and assay-based screening.[10–18] The rise of camera-based technologies has made digital imaging a practical substitute for spectrophotometers and other analytical tools, especially in point-of-need or cost-effective chemical analysis.[19–21] If not a replacement, camera-enabled analytics can serve as a bulk-level complement to more molecularly specific analyses.

Most digital cameras capture and store images in 8-bit sRGB format, a colour space originally proposed in 1996 by Microsoft and HP for consistency across CRT monitors and the Internet.[22] In 1999, sRGB became an official standard of the International Electrotechnical Commission as the default colour space for encoding and communicating RGB colours.[23] Figure 1 shows a representation of the 8-bit sRGB colour space as a cube of 16,777,216 colours. While suitable for consumer electronics, 8-bit sRGB was not designed for scientific purposes.

[a] Department of Pure and Applied Chemistry, University of Strathclyde, Glasgow G1 1XL, U.K.; E-mail: marc.reid.100@strath.ac.uk
[b] National Metrology Center (NMC), A*STAR, 8 Cleantech Loop, Singapore, 637145, Singapore

† Supplementary Information available. Beyond the supplementary information PDF, machine-readable data generated in this study can be found on figshare at: DOI: 00.0000/00000000.

View Article Online
DOI: 10.1039/D6DD00065G

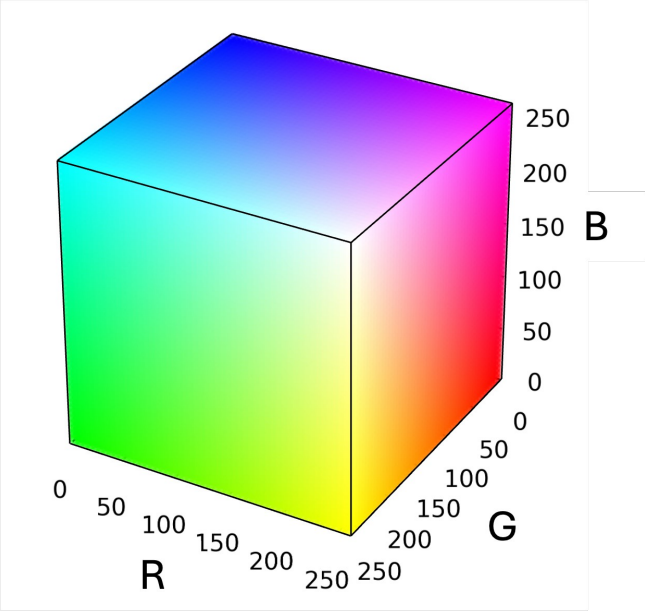

Fig. 1 The 8-bit sRGB colour space, consisting of 256 discrete levels in each of the three colour channels; Red, Green, and Blue. This 8-bit representation results in 16,777,216 ($2^8 \times 2^8 \times 2^8$) possible colour combinations. It is the default format for digital colour representation across most consumer imaging and display devices.

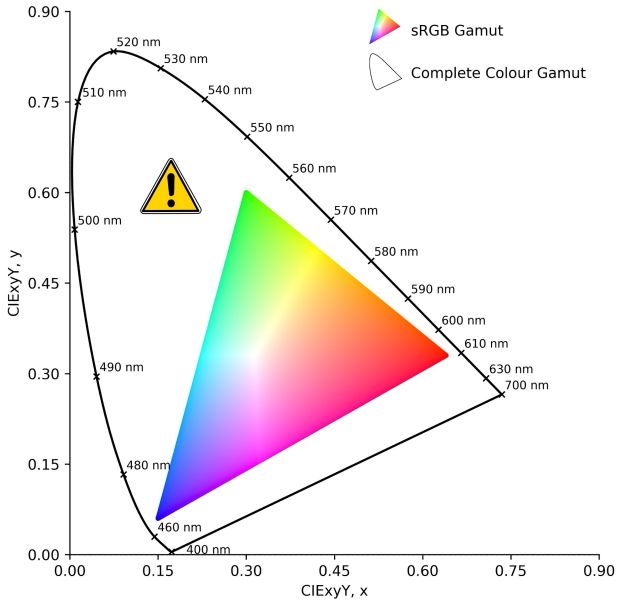

Fig. 2 CIE 1931 xy chromaticity diagram showing the complete colour gamut (horseshoe-shaped outline) encompassing all perceptible colours captured by typical human vision. The inner triangle represents the cross-sectional area of the 3D subset of colours that can be encoded using the 8-bit sRGB colour space, illustrating its limited coverage of the complete colour gamut.

The 8-bit sRGB space represents only a subset of colours defined by the Commission Internationale de l'Éclairage (CIE) 1931 colour system.[24] Chemicals that manifest highly saturated colours, such as dyes or transition metals, can lie outside the 8-bit sRGB gamut. Figure 2 shows the full CIE xy gamut, which captures all possible chromaticities. The region is bounded by the spectral locus curve, which corresponds to the 'pure' colour of the visible wavelengths. The ends of the curve are joined by a line (the 'line of purples') capturing the colours resulting from combining the wavelengths at the extremes (red and blue/violet). The subset of chromaticities covered by 8-bit sRGB corresponds to a triangle formed between the primary red, green, and blue that define it. The triangle itself is a 2D cross section of a 3D volume of colours not visible on the 2D projection of the gamut. When capturing a colour outside 8-bit sRGB subset, the camera device 'clips' the colour values to either 0 or 255, bringing them within the gamut, leading to information loss and distortion impacting scientific analysis, and potentially leading to chemical misinterpretation of the data.

The gamut limitations of 8-bit sRGB risk pronounced impact on chemical imaging and computer vision workflows. For example, two distinct chemical species or concentrations may thus (wrongly) map to the same 8-bit sRGB coordinates. In this work, we systematically investigate the impact of the 8-bit sRGB gamut constraints on camera-enabled process monitoring. We assess how colour information is distorted or lost during 8-bit sRGB encoding and explore the consequences for chemical interpretation of these data. Spectral data such as reflectance, transmittance, or emission can be converted to device-independent tristimulus CIE XYZ colour values. These spectral-derived CIE XYZ colour values can then be converted to 8-bit sRGB-encoded colours, providing a means to investigate and diagnose the impact of gamut clipping. Importantly, it must be stressed that gamut clipping represents a fundamental information *loss* rather than a correctable bias. Even perfectly calibrated cameras cannot recover colour information that lies outside the encoding gamut, distinguishing this limitation from more commonly discussed colour correction challenges.[25]

2 Methodology

2.1 Materials and dye preparation

Five common dyes were selected for this study: Blue 1, Red 40, Yellow 5, Yellow 6, and Crystal Violet (CV). Stock solutions (10 mM) of each dye were prepared. From these stock solutions, 16 samples were prepared by serial dilution into 3 mL, 10 mm pathlength cuvettes for spectral acquisition. The samples spanned six orders of magnitude, with concentration steps of 5, 3, and 1, resulting in samples ranging from 10 mM to 0.0001 mM, as shown

View Article Online
DOI: 10.1039/D6DD00065G

in Figure 3.

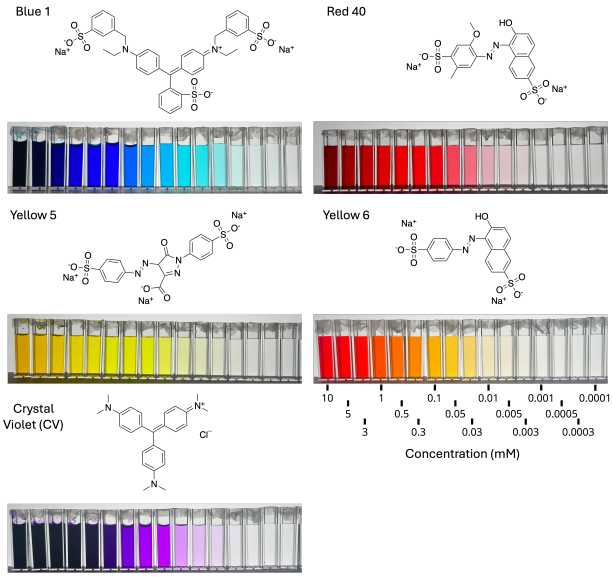

Fig. 3 Pictures of dye solutions and dye structures of Blue 1, Red 40, Yellow 5, Yellow 6, and Crystal Violet (CV). Dye solutions prepared over a range of concentrations, Left to right: 10 mM to 0.0001 mM in increments of 5, 3, and 1.

2.2 Spectral data acquisition

UV–vis transmission spectra were acquired for all 16 concentrations of each dye using a spectrophotometer (PerkinElmer LAMBDA 1050+ UV/Vis/NIR Spectrophotometer). Each spectrum was recorded from 360 to 830 nm.

2.3 Spectra to colour (CIE XYZ) conversions

Each transmission spectrum was then converted to CIE tristimulus values (X, Y, Z) using the CIE 1931 2° standard observer functions and the D65 illuminant. Conversions involve summing the product of the discrete wavelengths of the transmission data ($T(\lambda)$) with the standard illuminant spectra ($S(\lambda)$) and standard observer functions ($\bar{x}(\lambda),\bar{y}(\lambda),\bar{z}(\lambda)$). The 2° standard observer functions and D65 functions standard illuminant data were obtained from the CIE database at 1 nm resolution between 360 and 830 nm.[26–28] See Equation 1.

$$X = \frac{\sum_\lambda T(\lambda)S(\lambda)\bar{x}(\lambda)}{\sum_\lambda S(\lambda)\bar{y}(\lambda)} \quad Y = \frac{\sum_\lambda T(\lambda)S(\lambda)\bar{y}(\lambda)}{\sum_\lambda S(\lambda)\bar{y}(\lambda)} \quad Z = \frac{\sum_\lambda T(\lambda)S(\lambda)\bar{z}(\lambda)}{\sum_\lambda S(\lambda)\bar{y}(\lambda)} \tag{1}$$

2.4 Colour space conversions

The resulting tristimulus values were converted into the CIE xyY, 8-bit sRGB, and CIE L*a*b* colour spaces.[23,29]

In the following equations, we distinguish carefully between linear colour values and their non-linearly encoded (display-ready) counterparts. Lowercase symbols denote *linear* colour channel values, while uppercase symbols denote the corresponding *non-linearly encoded* values after sRGB *companding* (defined below).

Specifically, v represents a generic linear intensity value in the range $[0,1]$, prior to perceptual encoding. In the context of RGB colour channels, r, g, and b denote the linear red, green, and blue channel intensities obtained directly from the CIE XYZ to linear sRGB matrix transformation. These linear values are proportional to physical light intensity and are not yet suitable for direct 8-bit representation.

Uppercase R, G, and B represent the corresponding sRGB-encoded channel values after application of the sRGB companding function (IEC 61966-2-1), which introduces a controlled non-linearity to better match human visual perception of brightness. These encoded values are subsequently scaled to 8-bit integers in the range $[0,255]$ for analysis.

This distinction allows the equations below to explicitly separate physically linear colour information from perceptually encoded colour values, avoiding ambiguity when transitioning between colour spaces and bit depths.

- Equation 2: CIE XYZ to CIE xyY, chromaticity coordinates to plot on an xy chromaticity diagram.

$$x = \frac{X}{X+Y+Z} \quad y = \frac{Y}{X+Y+Z} \quad Y = Y \tag{2}$$

- Equations 3 to 5: CIE XYZ values were converted to standard 8-bit sRGB using the conventional colour-management pipeline: a matrix transformation from CIE XYZ to linear sRGB, followed by sRGB *companding* (the non-linear intensity mapping defined in the IEC 61966-2-1 standard that matches human brightness perception), and final scaling to 8-bit integer values.

$$\begin{bmatrix} r \\ g \\ b \end{bmatrix} = \begin{bmatrix} 3.2405 & -1.5371 & -0.4985 \\ -0.9693 & 1.8760 & 0.041556 \\ 0.0556 & -0.2040 & 1.0572 \end{bmatrix} \begin{bmatrix} X \\ Y \\ Z \end{bmatrix} \tag{3}$$

$$\begin{gathered} v \in r,g,b \\ V \in R,G,B \\ V = \begin{cases} 12.92v & \text{if } v \le 0.0031308 \\ 1.055v^{\frac{1}{2.4}} - 0.055 & \text{otherwise} \end{cases} \end{gathered} \tag{4}$$

$$\text{8-bit scaling} \begin{cases} 0 & \text{if V * 255} < 0 \\ 255 & \text{if V * 255} > 255 \\ \lfloor \text{V * 255} \rceil & \text{otherwise} \end{cases} \tag{5}$$

- Equation 6: To track overall colour change with a single, intuitive metric, we then calculated the RGB sum response (defined as the maximum possible sum R + G + B, 765, minus the measured R, G, and B values), providing a composite measure that captures changes across all three colour channels simultaneously.

$$RGB\ Sum\ Response = 765 - (R+G+B) \tag{6}$$

- Equations 7 and 8: Inverse 8-bit sRGB to CIE XYZ to investigate the 8-bit sRGB gamut clipping.

View Article Online
DOI: 10.1039/D6DD00065G

$$V \in R, G, B$$
$$v \in r, g, b$$
$$v = \begin{cases} \frac{V}{12.92} & \text{if } V \leq 0.04045 \\ (\frac{(V+0.055}{1.055})^{2.4} & \text{otherwise} \end{cases} \quad (7)$$

$$\begin{bmatrix} X \\ Y \\ Z \end{bmatrix} = \begin{bmatrix} 0.4124564 & 0.3575761 & 0.1804375 \\ 0.2126729 & 0.7151522 & 0.072175 \\ 0.0193339 & 0.119192 & 0.9503041 \end{bmatrix} \begin{bmatrix} r \\ g \\ b \end{bmatrix} \quad (8)$$

- Equations 9 and 10: Converting XYZ colour values to CIE L*a*b* colour space values, enabling calculation ΔE_{76} for measurement of colour difference between two colours:

$$L^* = 116 f(\tfrac{Y}{Y_n}) - 16$$
$$a^* = 500(f(\tfrac{X}{X_n}) - f(\tfrac{Y}{Y_n}))$$
$$b^* = 200(f(\tfrac{Y}{Y_n}) - f(\tfrac{Z}{Z_n}))$$
$$\text{where t is } \tfrac{X}{X_n}, \tfrac{Y}{Y_n}, or \tfrac{Z}{Z_n} \quad (9)$$
$$f(t) = \begin{cases} \sqrt[3]{t} & \text{if } t > \left(\frac{6}{29}\right)^3 \\ \frac{841}{108} t + \frac{4}{29} & \text{otherwise} \end{cases}$$
$$X_n = 95.0489,\ Y_n = 100,\ Z_n = 108.884 \text{ for D65}$$
$$\Delta E_{76} = \sqrt{(L_2^* - L_1^*)^2 + (a_2^* - a_1^*)^2 + (b_2^* - b_1^*)^2} \quad (10)$$

3 Results and discussion

3.1 Understanding and quantifying gamut clipping

Following the workflow outlined above, transmission spectra were first converted into CIE XYZ tristimulus values for all dye samples. These XYZ values represent a device-independent description of colour derived directly from the measured spectra. From the CIE XYZ values, several commonly used colour representations were then calculated, including CIE xyY chromaticity coordinates, CIE L*a*b* values, and 8-bit sRGB values. Full transmission spectra and spectra-to-colour conversions are provided in the supporting information.

To explicitly assess the impact of representing spectrally derived colours within the limited gamut of 8-bit sRGB, we then performed the reverse calculation: the 8-bit sRGB values were back-converted to CIE xyY chromaticity coordinates. This allowed direct comparison between:

(i) the original CIE xyY values obtained directly from the transmission spectra, and

(ii) the CIE xyY values reconstructed after conversion into, and back out of, the sRGB colour space.

Any divergence between these two sets of chromaticity coordinates arises from gamut clipping and quantisation effects introduced during the sRGB encoding step, rather than from the underlying spectral data itself. In this way, the magnitude and direction of colour distortion introduced by 8-bit sRGB encoding can be quantitatively assessed. The full conversion workflow and the resulting comparisons are shown in Fig. 4.

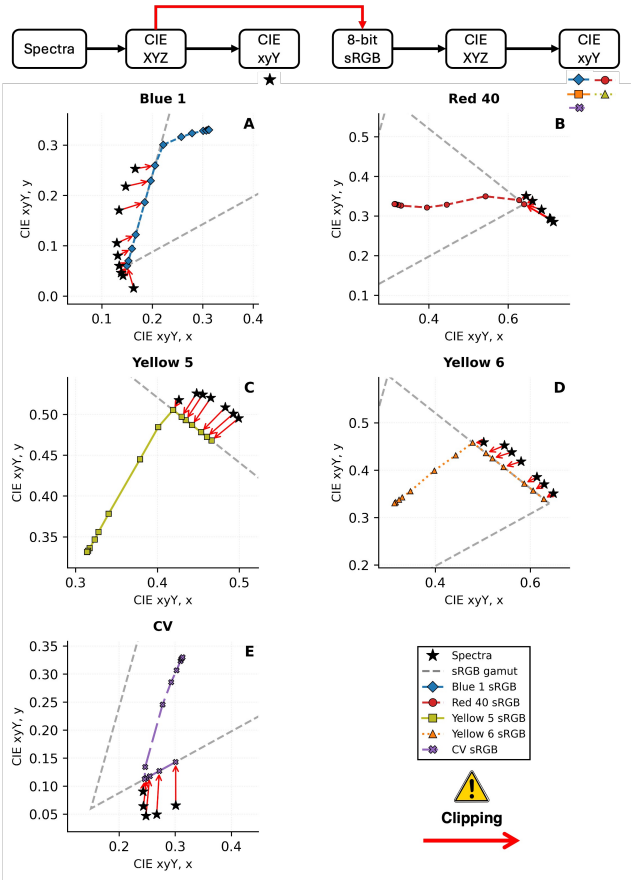

Fig. 4 Comparison of CIE xyY chromaticity coordinates derived from spectral measurements versus sRGB for Blue 1 (A), Red 40 (B), Yellow 5 (C), Yellow 6 (D), and Crystal Violet (E). Markers connected by lines represent sRGB-derived chromaticity coordinates at each concentration, while black stars indicate spectral chromaticity coordinates that fall outside the valid sRGB gamut [0, 255]. The grey dashed triangle delineates the sRGB colour gamut boundary. And red arrows connect out-of-gamut spectral coordinates to their corresponding clipped sRGB values.

Following the outermost points (those corresponding to the highest dye concentrations), the chromaticity coordinates move toward the region where all dyes converge at lower concentrations, namely the D65 white point ($x = 0.3127$, $y = 0.3290$). Across all dyes investigated, the data cross from outside to inside the 8-bit sRGB gamut; accordingly, gamut clipping occurs for many of the higher dye concentrations. This clipping is evident from data points lying on the boundary of the 8-bit sRGB triangle versus the corresponding back-calculated stars (from spectral measurements) that fall outside the 8-bit sRGB gamut (Fig. 4). The same back-calculation procedure can also be applied to spectral locus data to visualise how colours outside the 8-bit sRGB gamut are mapped onto the surface of the 8-bit sRGB space, as shown in the supporting information.

View Article Online
DOI: 10.1039/D6DD00065G

3.2 Tracking the impact of gamut clipping through colour difference measurements

Converting the CIE XYZ values to CIE L*a*b*, ΔE_{76} values can be calculated to quantify the colour differences due to gamut clipping. Fig. 5 summarises the values relevant to gamut clipping.

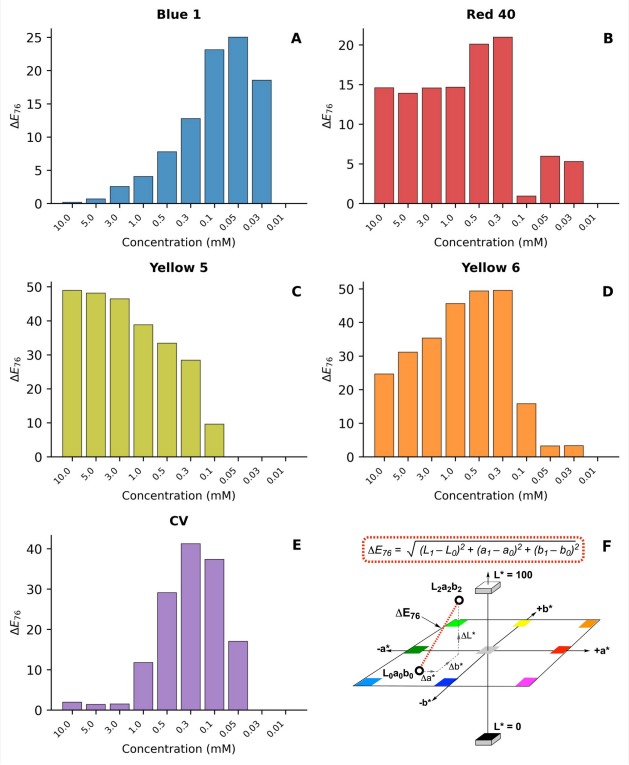

Fig. 5 Colour difference analysis comparing colours captured by the spectra and 8-bit sRGB. The ΔE_{76} values quantify the difference between spectra and 8-bit sRGB values due to gamut clipping for each dye, Blue 1 (A), Red 40 (B), Yellow 5 (C), Yellow 6 (D), and Crystal Violet (E). (F) A representation of the CIE L*a*b* colour space with ΔE_{76} exemplified.

Industry conventionally considers a ΔE_{76} value of 5 (and often lower) to represent the upper limit of acceptable colour mismatch in quality control.[30] In this context, ΔE_{76} provides a useful benchmark for assessing the perceptual significance of colour differences introduced by gamut clipping. All dyes investigated exhibited at least five samples with ΔE_{76} values exceeding 5, and all reached maximum values above $\Delta E_{76} = 20$. These large values arise for highly saturated colours lying outside the 8-bit sRGB gamut, where substantial differences are observed between colours derived directly from transmission spectra and those represented in sRGB.

For Yellow 5 and Yellow 6, ΔE_{76} values approach 50, corresponding to a visually extreme difference – comparable, for example, to the difference between a mid-grey (125, 125, 125) and white (255, 255, 255). By contrast, Blue 1 and CV show relatively low initial ΔE_{76} values (0.19 and 1.94, respectively), as their most concentrated solutions approach complete light absorption and therefore appear effectively black, minimising perceptual differences between spectral and sRGB representations. At concentrations below 0.01 mM, all dyes exhibit ΔE_{76} values below 0.01, indicating close agreement between spectral and 8-bit sRGB colour representations when the colours lie within the sRGB gamut. Notably, Red 40 and Yellow 6 display elevated ΔE_{76} values following the apparent transition back into the 8-bit sRGB gamut, highlighting residual distortions associated with prior gamut clipping.

To understand the elevated ΔE_{76} values, the 3rd dimension of the CIE xy chromaticity diagram needs to be considered. The CIE xy chromaticity diagram is a 2D projection of 3D data, CIE xyY. The increase in ΔE_{76} indicates that those colours lie outside the 8-bit sRGB gamut in the 3rd dimension, Y, the luminance (brightness). The 8-bit sRGB gamut in the CIE xyY colour space has a complex shape; the triangular projection, as seen from the xy plane of CIE xyY, has Y values across most of its range. Y values of the xy data all eventually converge at the white point, specifically the D65 white point (0.3127, 0.3290, 1) in CIE xyY or (255, 255, 255) in 8-bit sRGB. xY, and yY projections of the 8-bit sRGB gamut in CIE xyY are in the SI as well as interactive 3D plots. The contour plot in Fig. 6 shows the topology of the top surface of the 8-bit sRGB Gamut in CIE xyY.

View Article Online
DOI: 10.1039/D6DD00065G

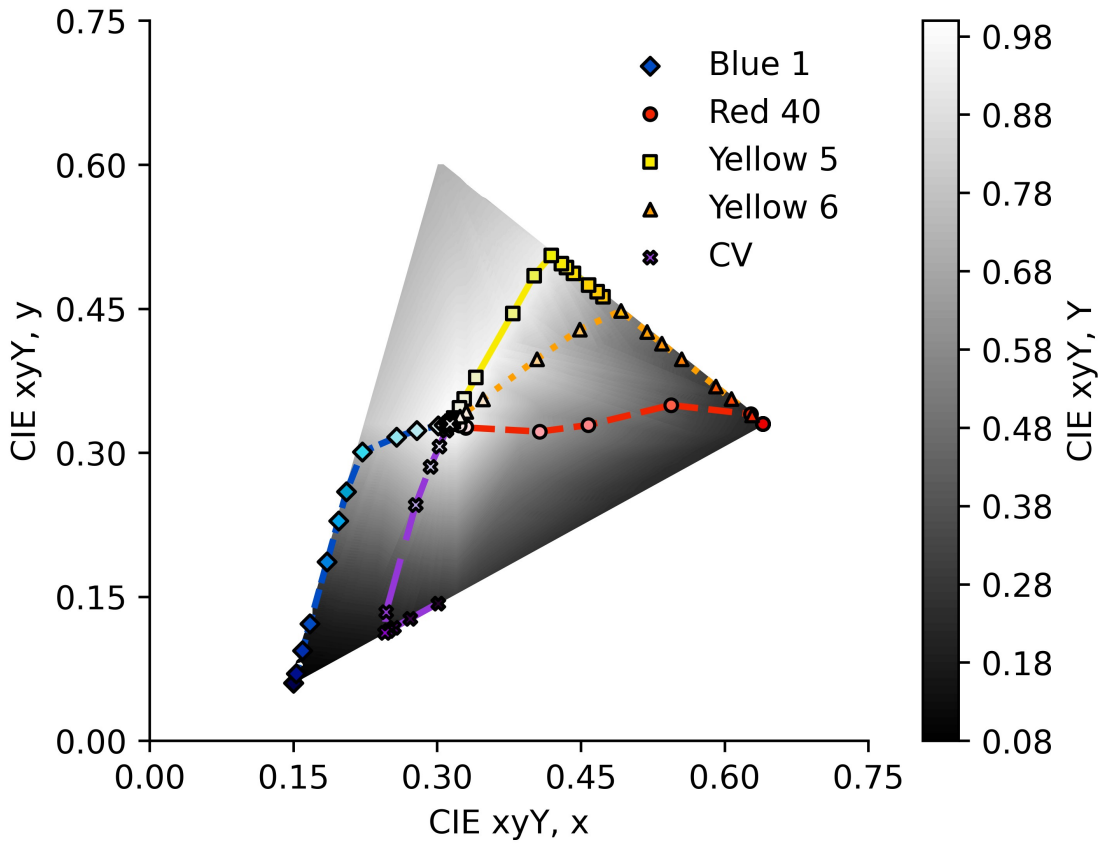

Fig. 6 CIE xy chromaticity plot, showing the 8-bit sRGB gamut with grayscale contours corresponding to the maximum Y value for given xy coordinates. The paths and appropriately coloured points show the 5 dyes series as captured in 8-bit sRGB and how they change in brightness.

Gamut clipping is a result of the conditionals associated with Eqn. 5. Any acquired RGB data containing 0 or 255 values is at the limits of the 8-bit sRGB colour space, and such values are likely the result of gamut clipping. As the 8-bit sRGB data presented has been derived from transmission spectra via CIE XYZ colour values, the clipping conditionals of Eqn. 5 can be skipped to determine the hypothetical sRGB values required to represent the true colour beyond the 256 possible values for each channel. Fig. 7 summarises these data, showing that gamut clipping affected all five compounds, with violations occurring in both directions beyond the 0 to 255 8-bit sRGB range. Negative clipping (R, G, or B values that are negative are set to zero), in particular, is prominent for all compounds, with negative values in at least one of the R, G, or B channels. Negative values indicate that the true colour is a 'purer' colour than encoded, with complete absorption of some visible wavelengths. Positive clipping was less extreme but still significant. Red 40, Yellow 5, and Yellow 6 all exceeded 255 by up to 22 units in the R channel. Values above 255 correspond to a colour brighter or more luminous than 8-bit sRGB can encode.

View Article Online
DOI: 10.1039/D6DD00065G

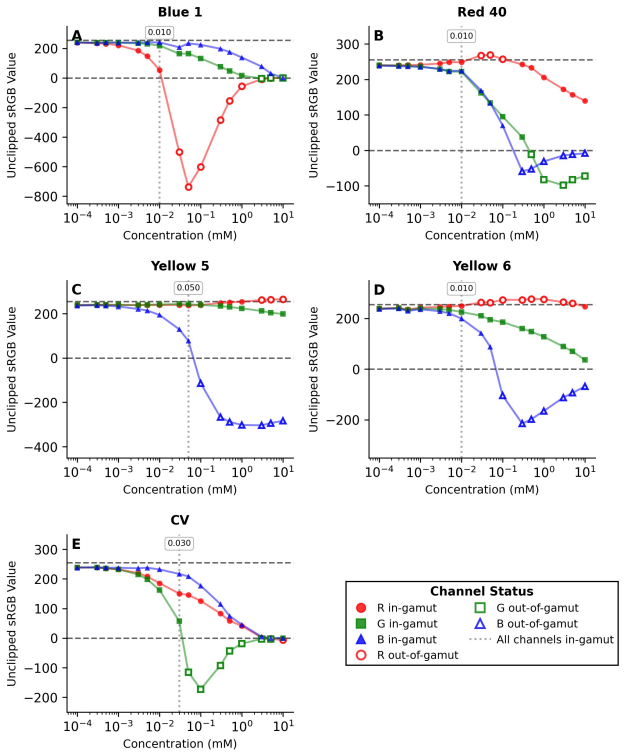

Fig. 7 Unclipped sRGB values for Blue 1 (A), Red 40 (B), Yellow 5 (C), Yellow 6 (D), and Crystal Violet (E). Each panel shows unclipped red (circles), green (squares), and blue (triangles) channels as a function of concentration. Filled markers indicate values within the valid 8-bit sRGB range [0, 255] (in-gamut), while open markers indicate values outside this range (out-of-gamut) that would be subject to clipping. Horizontal dashed lines mark the 0 and 255 boundaries of the sRGB colour space. Vertical dotted lines indicate the highest concentration at which all three RGB channels are simultaneously in-gamut, with the concentration value shown in the label (mM). Highlighting the significant information loss that occurs due to gamut clipping.

3.3 The impact of 8-bit sRGB gamut clipping on process monitoring, theoretical 1st order decay trends

Previously, we reported a discontinuity in the RGB-derived metric, RGB sum response, during an investigation of the pseudo-first-order decay of Blue 1 using sodium percarbonate, as part of colour calibration strategies for video data between smartphones.[25] This serendipitous discovery of discontinuity in the camera-recorded colour profile was a result of gamut clipping, resulting in 'shouldering' in the kinetic profile and thus two distinct trends.

With samples spanning several orders of concentration magnitude, and assuming a first-order decay of the dyes, theoretical colour time-series data can be generated. This approach enables the investigation of how the sRGB gamut limitations may manifest in colour-based reaction monitoring. Because the data are derived from spectra, it is isolated from critical external factors, such as device-dependent processing or lighting which each influence camera data. Given the variety of ways to transform colour data, various colour metrics have been used for process monitoring in chemistry, from single colour channels to derived metrics. This work focused on two derived metrics, the RGB sum response (Equation 6) and ΔE_{76} (Equation 10). Time points for the decay were determined based on the solution concentrations and an assumed first-order rate constant of 1 s^{-1}. Theoretical first-order decay trends are shown in Figure 8 and Figure 9 for RGB sum response, and ΔE_{76}, respectively.

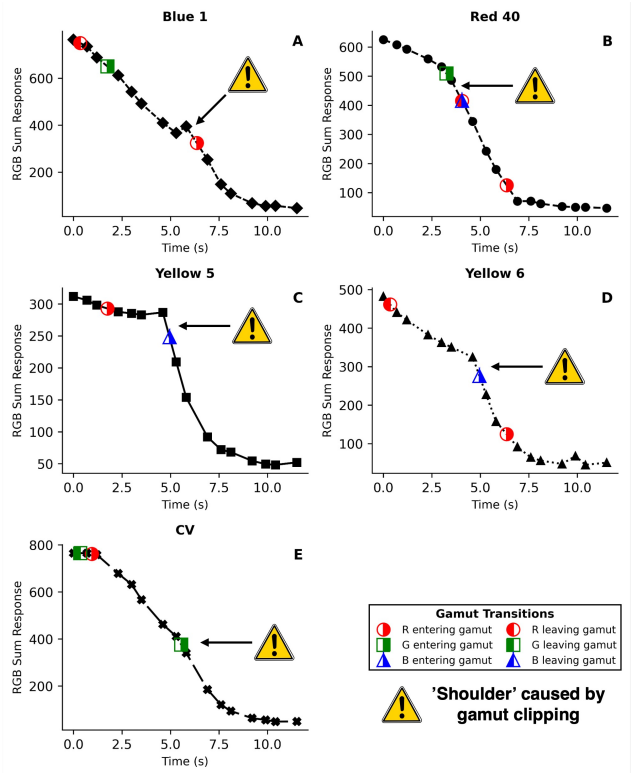

Fig. 8 RGB sum response (765-(R+G+B)) time series data for theoretical first-order decay (assumed rate constant k=1 s^{-1}) for Blue 1 (A), Red 40 (B), Yellow 5 (C), Yellow 6 (D), and Crystal Violet (E). Each panel shows RGB sum response (765 − R − G − B) calculated from spectra-derived sRGB data. Half-filled markers indicate gamut transitions for individual RGB channels, with the fill direction encoding transition type: right-filled markers denote channel entry into the valid sRGB gamut [0, 255], while left-filled markers indicate channel exit from the valid range. Transitions correspond to key points in the time series data.

Visual detection of gamut clipping using RGB Sum Response

Two distinct trends are clear in RGB sum response plots: first, a gradual decrease followed by a 'shoulder-like' trend break when transitioning from outside to inside the 8-bit sRGB gamut, after which there is a more rapid decrease over time. Without the context, such profiles could be misinterpreted as having two distinct phases, but in reality (as determined through pure spectroscopic means), it is only one. Blue 1 and CV exhibit early shouldering transitions; the solutions are close to total absorption and appear almost completely black at these transitions. The unclipped values in these instances are very close to the valid range and have minimal impact on the trends. But in each case, a channel leaves and then enters, causing a trend break (i.e. shouldering).

Any gamut transitions caused by clipping values above 255 have minimal impact on the trends. However, clipping of negative values all correspond to trend breaks in the RGB sum re-

View Article Online
DOI: 10.1039/D6DD00065G

sponse plots.

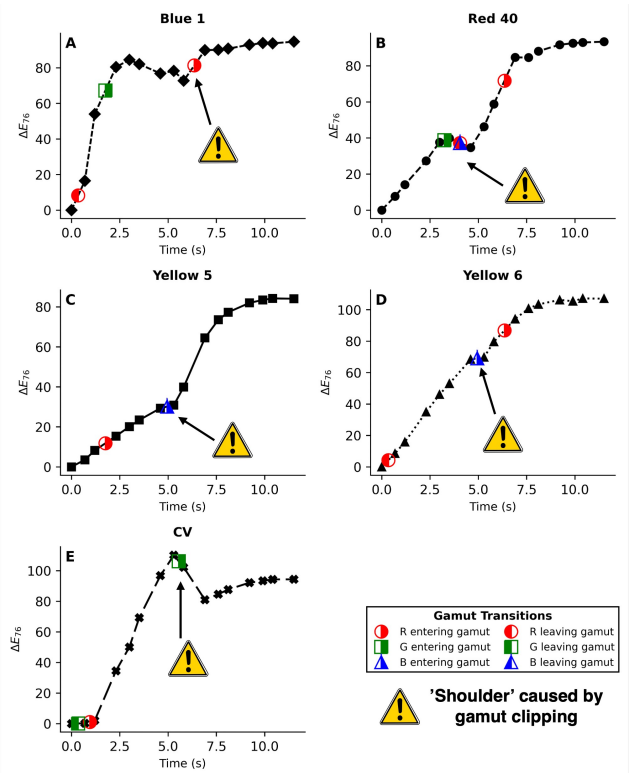

Fig. 9 ΔE_{76} time series data for theoretical first-order decay (assumed rate constant k=1 s^{-1}) for Blue 1 (A), Red 40 (B), Yellow 5 (C), Yellow 6 (D), and Crystal Violet (E). Each panel shows ΔE_{76} calculated from spectra-derived sRGB data. Half-filled markers indicate gamut transitions for individual RGB channels, with the fill direction encoding transition type: right-filled markers denote channel entry into the valid sRGB gamut [0, 255], while left-filled markers indicate channel exit from the valid range. Transitions correspond to key points in the time series data.

Visual detection of gamut clipping using ΔE

In the ΔE_{76} plots, again, the gamut transitions again appear as artefacts in the profiles. Transitions that previously corresponded to trend breaks now correspond to inflection points in Red 40, Yellow 5, and Yellow 6. The CV and Blue 1 ΔE_{76} profiles are unique. For Blue 1, the key transition is followed by a level break in the time-series data. And by the ΔE_{76} metric, Blue 1 would appear to plateau much earlier than the others. For CV, the gamut transition is followed by a decrease in the data. ΔE_{76} is a comparative metric; it needs a reference point, the decrease indicates that the colour is moving closer to the reference. For these data, the reference is the colour of the 10 mM sample for each dye. The reference can therefore influence the trajectory of time-series data. Even if concentration is always decreasing, the trajectory of the colour values doesn't necessarily make that clear, especially for solutions that start very dark, like CV. They follow a more parabolic path in the colour space from the dark starting point, passing through a more vivid colour(s), then to white/clear.

A first-order rate constant of k = 1 s^{-1} was chosen for convenience. These data could have been generated with any rate constant, and the trends would remain unchanged. The relative temporal spacing between data points is unchanged because the concentration ratios remain the same and the time axis scales linearly with 1/k. Gamut-clipping artefacts depend solely on the sequence of concentrations traversed during decay, not on the rate at which they are traversed. Thus, the observed discontinuities occur at the same concentration transitions regardless of the rate constant. The findings, therefore, apply to camera-based monitoring across all reaction timescales. The exact concentration at which gamut clipping occurs will vary depending on the capture environment and equipment.

3.4 A practical example of gamut clipping in camera data

Crystal violet hydroxylation, mediated by an excess of aqueous sodium hydroxide, was monitored in a Duran bottle using a commercial camcorder. Full experimental and setup details are included in the supporting information. The video recording was then analysed using *Kineticolor*, a computer vision software developed bin our team for process monitoring.[31] We thus extracted the 8-bit sRGB values from a selected region in the Duran bottle for each second of the video, providing average 8-bit sRGB values. These values were then converted to several other colour spaces, including reporting ΔE_{76} values, using the data in the first video frame as the reference against which to measure subsequent colour differences. The RGB sum response was calculated for each time point from the average 8-bit sRGB values using Equation 6. RGB Sum response and ΔE_{76} time series plots are shown in Fig. 10.

At a starting concentration of 0.05 mM (and a pathlength greater than 10 mm), CV is outside the 8-bit sRGB gamut, as captured in the video. Gamut clipping of the green channel is evident from the 0 values, indicating true values were negative and unpresentable in sRGB space. A clear trend break occurs when the green channel enters the gamut between 80 and 81 s as indicated by the green dashed line. The trends follow the previous discussion of the theoretical first-order trends in Fig. 8 and Fig. 9 for RGB sum response and ΔE_{76}, respectively. RGB sum response shows two distinct trends before and after the transition, and ΔE_{76} corresponds to the turning point of the ΔE_{76} data. This practical example illustrates that the gamut clipping issues identified in our concentration-series analyses (Fig. 8 and Fig. 9) are not merely theoretical concerns but manifest as systematic errors in real experimental workflows.

3.5 Broader implications

The limitations of 8-bit sRGB extend beyond distorted kinetics to affect multiple aspects of digital chemistry workflows. As camera-based chemical analysis becomes increasingly integrated into automated workflows, high-throughput screening, machine-learning pipelines, and process analytical tools, understanding these constraints is critical to ensuring data quality, reproducibility, and reliable decision-making. Models trained on 8-bit sRGB data will inherit the non-linearities and discontinuities introduced by gamut clipping. Unique samples may map to identical 8-bit sRGB values, making them indistinguishable to classification or regression algorithms. The discontinuities introduced by gamut

View Article Online
DOI: 10.1039/D6DD00065G

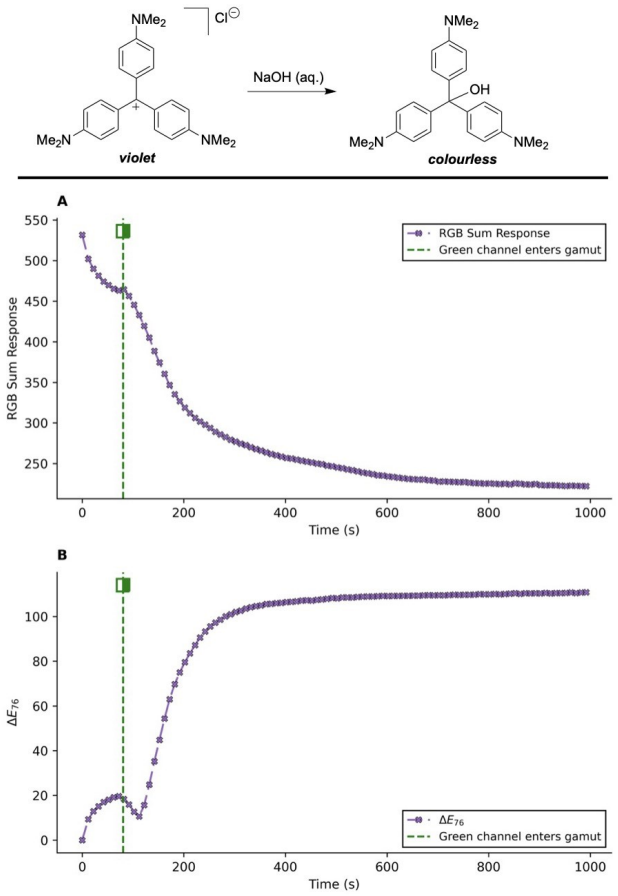

Fig. 10 A practical example of gamut clipping in camera-based monitoring of Crystal Violet degradation using excess sodium hydroxide, showing (A) RGB Sum Response (765-(R+G+B)) and (B) ΔE_{76}. The green dashed line and half-filled square between 80 and 81 s mark where the green channel enters the valid 8-bit sRGB gamut [0, 255].

clipping violate the assumption of a continuous relationship underlying many calibration models. In systems with multiple chromophores, gamut clipping can affect each species differently, potentially distorting their relative contributions to the overall colour.

Additionally, we have used a single pathlength to study the effect of gamut clipping, where computer vision is being applied in chemistry; the typical pathlength when observing through common glassware is greater than that of a 10 mm cuvette. Saggiomo *et al.* have reported a variable pathlength cell; such a device could be useful for exploring the impact of pathlength on gamut clipping.[32]

3.6 Practical guidance for researchers

3.6.1 Detecting gamut clipping

Before beginning an experiment, perform a simple visual inspection: compare the sample as seen directly with its appearance on the camera's digital display. First, calibrate the capture equipment using a reference within the gamut, such as colour calibration charts, to ensure faithful reproduction of the reference on the capture device's display. If the sample appears more vivid, saturated, or brighter in person than on screen, gamut clipping may be occurring and should be verified numerically via channel histograms. When processing images/videos, researchers should check for RGB values at the extremes (0 or 255) as an indicator that samples are too 'colourful' for 8-bit sRGB. A recommended workflow is shown in Fig. 11.

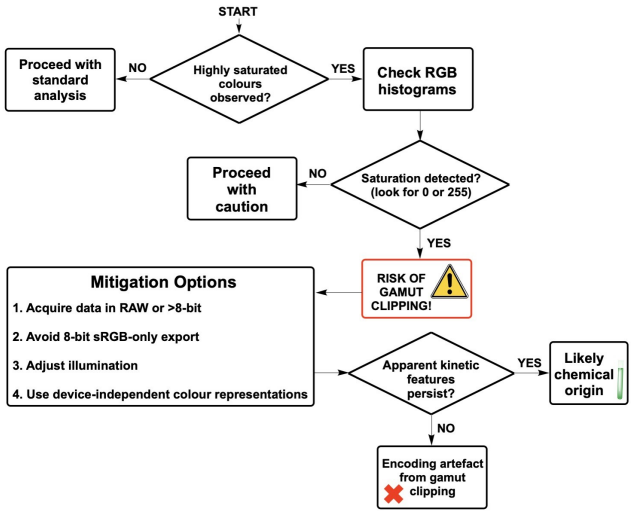

Fig. 11 Practical workflow for diagnosing and mitigating colour gamut clipping in camera-based chemical analysis. Saturated colours can lead to channel saturation in 8-bit sRGB encoding, introducing artificial features into time-series data that may be misinterpreted as chemical kinetics.

Alternative colour spaces

When clipping is detected, consider capturing data in wider-gamut colour spaces. Many modern cameras support the wider gamut of DCI-P3 or capture in RAW and process in Adobe RGB (1998) or ProPhoto RGB, which encompass significantly more colours than sRGB. Also consider a camera with increased bit depth per channel, preserving information that would otherwise be lost in 8-bit encoding, providing greater sensitivity for subtle colour changes. The extent of each wider gamut's is shown in the CIE xy chromaticity plot in Fig. 12.[33–36]

View Article Online
DOI: 10.1039/D6DD00065G

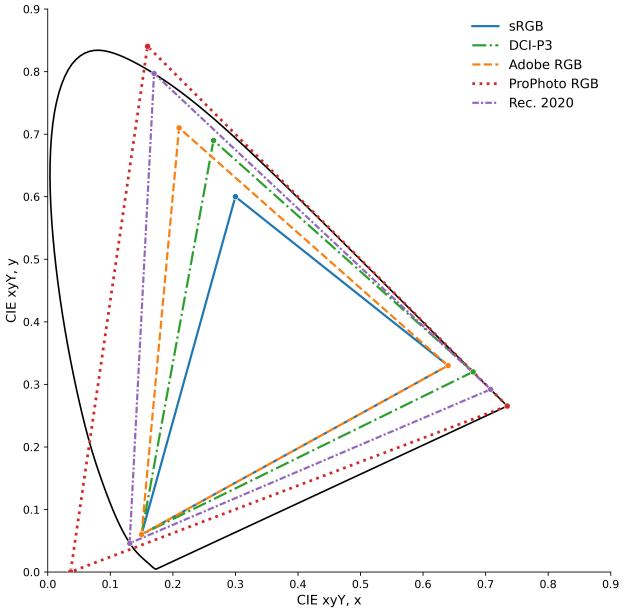

Fig. 12 RGB colour space gamut comparison on the CIE 1931 xy chromaticity diagram. The spectral locus (black curve) represents all visible colours. Triangular gamuts show the colour reproduction capabilities of sRGB, Adobe RGB, DCI-P3, ProPhoto RGB, and Rec. 2020 encoding standards. All provide wider gamuts than the standard sRGB space.

Sharing standards

To ensure reproducibility, researchers should explicitly document: i) the colour space used (sRGB, DCI-P3, etc.), ii) bit depth, iii) whether values are gamma-corrected or linear, iv) illumination conditions (light source type and colour temperature), and v) any image processing applied. When possible, deposit the original unprocessed image/video files in repositories to enable reanalysis and validation by others.

Conclusions

This study critically evaluated the limitations of the 8-bit sRGB colour space in representing chemically relevant colour data captured via digital imaging. Using experimental dye series and theoretical colourimetric time-series plots, we demonstrated that saturated or bright colours can fall outside the 8-bit sRGB gamut, leading to colour distortion, discontinuities, and non-linear visual representations.

By converting visible transmission spectra into CIE tristimulus values (XYZ) and then to 8-bit sRGB, we quantified how encoding affects the perceived colour change across a range of concentrations. Theoretical kinetic trends further revealed that these encoding artefacts can obscure true reaction dynamics, and that gamut transitions correspond to structural breaks (trend and level breaks) in the data.

As with all camera-based colour measurements, the recorded pixel values reflect the combined effect of transmitted, reflected, and scattered light reaching the sensor, such that observed gamut excursions arise from the full optical scene rather than transmission alone. Accordingly, the risks identified here apply to any optical scene in which the colour trajectory crosses an encoding gamut boundary, irrespective of whether the dominant contribution is transmission, reflection, or scattering.

Spectrum-to-colour offers a reproducible and objective benchmark for validating digital colour measurements. Addressing these limitations is essential to ensure the integrity of digital chemistry pipelines and their integration into broader applications and workflows. Raw imaging formats, proper calibration, or hardware with wider gamuts should be investigated.

Author contributions

C.F.: conceptualisation; methodology; data curation; formal analysis; software; visualisation; writing (original draft).
S.Y.: resources; funding acquisition; supervision.
M.R.: resources; conceptualisation; writing (review & editing); supervision; project administration; funding acquisition.

Conflicts of interest

MR is the inventor of Kineticolor and leading the software commercialization process. For information on licensing Kineticolor software, please contact the corresponding author and the University of Strathclyde technology transfer office:
marc.reid.100@strath.ac.uk; iprmanager@strath.ac.uk

Data availability

Both Excel and Python were used to perform the calculations and visualisations generated in this paper. In addition to the higher-level details shared in the supporting information PDF document, a zipped folder of machine-readable data and scripts, ordered according to the Figure numbers in the main text, is available on 'figshare' at: `https://doi.org/10.6084/m9.figshare.31268116`

Acknowledgements

CF and MR thank Singapore's Agency for Science, Technology and Research (A*STAR) for PhD funding support through A*STAR Research Attachment Programme (ARAP). Any opinions, findings and conclusions or recommendations expressed in this material are those of the author(s) and do not reflect the views of A*STAR. MR thanks the UK Research and Innovation for Future Leaders Fellowship funding (MR/T043458/1).

References

1 L. F. Capitán-Vallvey, N. López-Ruiz, A. Martínez-Olmos, M. M. Erenas and A. J. Palma, *Analytica Chimica Acta*, 2015, **899**, 23–56.
2 G. M. Fernandes, W. R. Silva, D. N. Barreto, R. S. Lamarca, P. C. F. Lima Gomes, J. Flávio da S Petruci and A. D. Batista, *Analytica Chimica Acta*, 2020, **1135**, 187–203.
3 M. A. Gaidimas, A. Mandal, P. Chen, S. X. Leong, G.-H. Kim, A. Talekar, K. O. Kirlikovali, K. Darvish, O. K. Farha, V. Bernales and A. Aspuru-Guzik, *Digital Discovery*, 2026.
4 A. A. Boulgakov, S. R. Moor, H. H. Jo, P. Metola, L. A. Joyce, E. M. Marcotte, C. J. Welch and E. V. Anslyn, *The Journal of Organic Chemistry*, 2020, **85**, 9447–9453.
5 Y. Li, B. Dutta, Q. J. Yeow, R. Clowes, C. E. Boott and A. I. Cooper, *Digital Discovery*, 2025, **4**, 1276–1283.

View Article Online
DOI: 10.1039/D6DD00065G

6 C. Yan, M. Cowie, C. Howcutt, K. M. P. Wheelhouse, N. S. Hodnett, M. Kollie, M. Gildea, M. H. Goodfellow and M. Reid, *Chem. Sci.*, 2023, **14**, 5323–5331.

7 R. El-khawaldeh, M. Guy, F. Bork, N. Taherimakhsousi, K. N. Jones, J. M. Hawkins, L. Han, R. P. Pritchard, B. A. Cole, S. Monfette and J. E. Hein, *Chemical Science*, 2024, **15**, 1271–1282.

8 Y.-F. Gao, D. Meng, X.-Y. Li, S.-H. Wang, J.-X. Chen, R.-Y. Cao, Y.-T. Zhai, J.-E. Hu, Q.-L. Bai, Z.-P. Zhang, Y.-Y. Li, K. Li and S.-Q. Zang, *Journal of Chemical Education*, 2025, **102**, 2436–2442.

9 H. Barrington, T. J. D. McCabe, K. Donnachie, C. Fyfe, A. McFall, M. Gladkikh, J. McGuire, C. Yan and M. Reid, *Angewandte Chemie International Edition*, 2024, **64**, e202413395.

10 N. R. Murray, T. J. D. McCabe, M. Reid and E. R. Draper, *J. Mater. Chem. C*, 2024, **12**, 12483–12490.

11 C. Yan, C. Fyfe, L. Minty, H. Barrington, C. Jamieson and M. Reid, *Chem. Sci.*, 2023, **14**, 11872–11880.

12 H.-L. Wei, X.-M. Ma, J.-Z. Qin, Y.-H. Su and Z.-H. Luo, *Chemical Engineering Science*, 2026, **320**, 122720.

13 C. Fyfe, H. Barrington, C. M. Gordon and M. Reid, *Organic Process Research & Development*, 2024, **28**, 3661–3673.

14 C. Fyfe, R. Duncan, T. J. D. McCabe, K. Donnachie, H. Barrington and M. Reid, *ACS Sustainable Chemistry & Engineering*, 2025, **13**, 17241–17256.

15 N. Bugeja, C. Oliver, N. McGrath, J. McGuire, C. Yan, F. Carlysle-Davies and M. Reid, *Digital Discovery*, 2023, **2**, 1143–1151.

16 L. Wang and Z. Zhang, *Sensors and Actuators B: Chemical*, 2008, **133**, 40–45.

17 W. Zhu, H. Xie, X. Yue, N. Li, Z. Hu, B. Liu and J. Zhang, *Microchemical Journal*, 2025, **218**, 115653.

18 Y. Han, I. Borne, B. Dutta, R. Clowes, H. Qu, A. James, C. E. Boott, M. A. Little and A. I. Cooper, *Angewandte Chemie*, 2025, **137**, e202510400.

19 S. Smolders, H. Sheng, M. P. Mower, A. Potdar and J. Dijkmans, *Organic Process Research & Development*, 2023, **27**, 1339–1347.

20 V. Markus, A. A. Paul, R. S. Marks and J. Caleb, *Analytical Letters*, 2026, **59**, 158–176.

21 L. S. V. Barbosa, P. Strauch, D. C. M. B. Santos, M. G. A. Korn and R. M. M. Santana, *Journal of Chemical Education*, 2023, **100**, 2601–2607.

22 M. Anderson, R. Motta, S. Chandrasekar and M. Stokes, *Color and Imaging Conference*, 1996, **4**, 238–238.

23 *Multimedia systems and equipment – Colour measurement and management – Part 2-1: Colour management – Default RGB colour space – sRGB*, 1999.

24 T. Smith and J. Guild, *Transactions of the Optical Society*, 1931, **33**, 73.

25 C. Fyfe, S. Yu, J. Zhang and M. Reid, *Analytical and Bioanalytical Chemistry*, 2025, **417**, 5753–5770.

26 I. C. on Illumination (CIE), *Colour-matching functions of CIE 1931 standard colorimetric observer*, 2019.

27 I. C. on Illumination (CIE), *CIE standard illuminant D65*, 2019.

28 E. Committee, *Practice for Computing the Colors of Objects by Using the CIE System*, 2022.

29 E. Carter, J. Schanda, R. Hirschler, D. Jost, M. Luo, M. Melgosa, Y. Ohno, M. Pointer, D. Rich, F. Viénot, L. Whitehead and J. Wold, *CIE 015:2018 Colorimetry, 4th Edition*, International Commission on Illumination, Vienna, 2018.

30 R. McDonald, *Colour Physics for Industry*, Society of Dyers and Colourists, Bradford, West Yorkshire BD1 2JB, 1997, p. 156.

31 M. Reid, in *Chapter Three - Computer vision for mixing analysis: Transforming cameras into quantitative tools for chemical process understanding*, ed. N. H. Williams and J. B. Harper, Academic Press, 2025, vol. 59, pp. 65–119.

32 X. Liu, N. Sharma, A. H. Velders and V. Saggiomo, *Digital Discovery*, 2025, **4**, 3238–3244.

33 *D-cinema quality - reference projector and environment*, 2011.

34 *Multimedia systems and equipment - Colour measurement and management - Part 2-5: Colour management - Optional RGB colour space - opRGB*, 2007.

35 *Photography and graphic technology — Extended colour encodings for digital image storage, manipulation and interchange Part 2: Reference output medium metric RGB colour image encoding (ROMM RGB)*, 2013.

36 *Parameter values for ultra-high definition television systems for production and international programme exchange*, 2015.

View Article Online
DOI: 10.1039/D6DD00065G

When Chemistry is Too Colourful: Gamut Clipping in 8-bit sRGB Risks Misinterpretation of Camera-Based Chemical Analysis

Both Excel and Python were used to perform the calculations and visualisations generated in this paper. In addition to the higher-level details shared in the supporting information PDF document, a zipped folder of machine-readable data and scripts, ordered according to the Figure numbers in the main text, is available on 'figshare' at: https://doi.org/10.6084/m9.figshare.
31268116

Marc Reid
marc.reid.100@strath.ac.uk